In situ generation of zinc oxide nanobushes on microneedles as antibacterial coating

Chew, Sharon Wan Ting; Zeng, Yongpeng; Cui, Mingyue; Chang, Hao; Zheng, Mengjia; Wei, Shi; Zhao, Wenting; Xu, Chenjie

2019

Chew, S. W. T., Zeng, Y., Cui, M., Chang, H., Zheng, M., Wei, S., ... Xu, C. (2019). In situ generation of zinc oxide nanobushes on microneedles as antibacterial coating. SLAS Technology, 24(2), 181-187. doi:10.1177/2472630318812350

https://hdl.handle.net/10356/146338

https://doi.org/10.1177/2472630318812350

In Situ Generation of Zinc Oxide Nanobushes on Microneedles as Antibacterial Coating

Sharon W. T. Chew[1,2], Yongpeng Zeng[2], Mingyue Cui[2,3], Hao Chang[2], Mengjia Zheng[2], Shi Wei[4], Wenting Zhao[2], and Chenjie Xu[1,2,3]

Abstract

This paper introduces a facile and scalable method to generate a layer of antibacterial coating on microneedles. The antibacterial coating (i.e., zinc oxide nanobushes) is generated on the surface of gold-coated polystyrene microneedles using the hydrothermal growth method. The antimicrobial property is examined using the agar diffusion test with both gram-positive and gram-negative bacteria.

Keywords

zinc oxide nanobushes, antibacterial coating, microneedles, skin

Introduction

Microneedles (MNs) containing arrays of miniaturized needles of microscale length are promising platform technologies for transdermal drug delivery and biosensing applications due to their ability to perforate the skin barrier in an almost painless and minimally invasive manner.[1–3] While enormous success has been reported for transdermal delivery of drugs and vaccines,[4–6] one concern is that the MN-generated microchannels might result in bacterial infection.[7] The stratum corneum layer acts as the outermost protective barrier that prevents foreign materials, including microorganisms, from entering the body. Microchannels generated by MNs could result in pathogenic microorganisms such as *Staphylococcus aureus*, which reside on the skin surface, entering the body and causing infection.[8]

To address this, one idea is to fabricate MNs or coat MNs with antimicrobial materials. For example, two-photon polymerization micromolding was used to fabricate MNs containing gentamicin, an antimicrobial agent.[9–11] Materials with antimicrobial properties have also been incorporated during the fabrication process to give MNs their antimicrobial properties.[12,13] However, all these methods for the fabrication of antimicrobial MNs are too complicated and difficult for upscaling. And for certain antimicrobial agents, it is still unclear if the agents will exhibit any immunogenic behavior in in vivo applications.[12]

This paper proposes a facile and scalable method to generate a layer of antibacterial coating on the MN surface. Specifically, as shown in **Figure 1**, zinc oxide (ZnO) nanobushes were deposited on the surface of gold-coated (Au-coated) polystyrene (PS) MNs using the hydrothermal growth method. The morphology and density of ZnO nanobushes were influenced by the concentration of precursors. Antimicrobial property was examined using the agar diffusion test with gram-positive bacteria (i.e., *S. aureus* ATCC 15981) and gram-negative bacteria (i.e., *Salmonella enterica* subsp. *enterica*). This strategy can also be extended

[1]NTU Institute for Health Technologies, Interdisciplinary Graduate School, Nanyang Technological University, Singapore
[2]School of Chemical and Biomedical Engineering, Nanyang Technological University, Singapore
[3]Nanyang Environment & Water Research Institute, Nanyang Technological University, Singapore
[4]Key Laboratory of Flexible Electronics (KLOFE) and Institute of Advanced Materials (IAM), Nanjing Tech University, Nanjing, Jiangsu, China

Received Aug 22, 2018, and in revised form Oct 10, 2018. Accepted for publication Oct 20, 2018.

Corresponding Authors:
Chenjie Xu, NTU Institute for Health Technologies, Interdisciplinary Graduate School, Nanyang Technological University, 62 Nanyang Drive, Singapore, 637459, Singapore.
Email: cjxu@ntu.edu.sg

Wenting Zhao, School of Chemical and Biomedical Engineering, Nanyang Technological University, 62 Nanyang Drive, Singapore 637459, Singapore.
Email: wtzhao@ntu.edu.sg

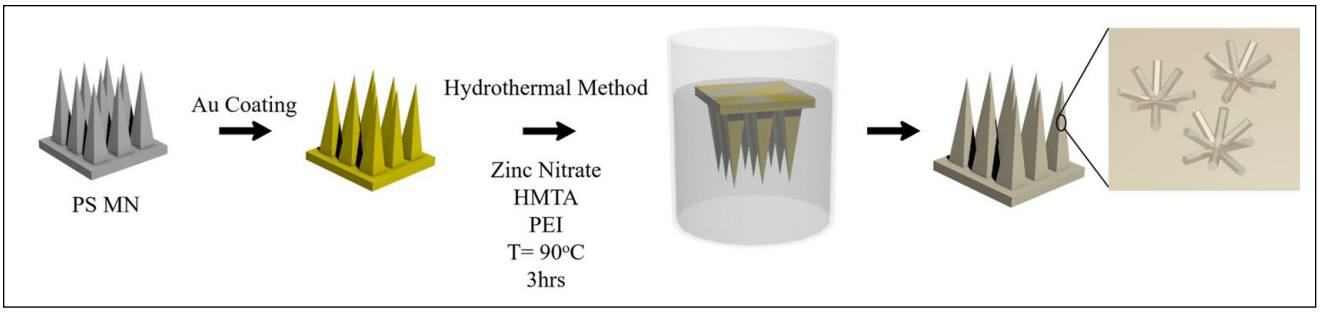

Figure 1. Schematic of ZnO nanobush generation on Au-coated PS MNs via hydrothermal growth method.

to generate similar submicron features on MNs made of other materials, which could potentially fine-tune the drug release profile, the mechanical property, and the surface property of the MN devices.

Experimental

Fabrication of PS MNs

PS MNs were fabricated via micromolding using polydimethylsiloxane (PDMS) negative molds. The PDMS negative mold was prepared by pouring PDMS (10:1 w/w ratio of prepolymer base to curing agent, Dow Corning, Midland, MI) over the stainless steel MN master structure (Micropoint Technologies, Singapore), followed by degassing in a vacuum oven for 10 min and curing at 70 °C for 1 h. PS resins were then placed into the plasma-treated PDMS negative molds and heated at 240 °C in vacuum conditions for 45 min. Subsequently, after cooling down to room temperature, PS MNs were gently removed from the PDMS molds.

Deposition of ZnO Nanobushes on PS MNs via Hydrothermal Growth Method

PS MNs were precoated with a 10 nm thick gold film using the thermal evaporation (UNIVEX 250 Benchtop, Leybold, Cologne, Germany). ZnO nanobushes were generated on the Au-coated PS MNs in a hydrothermal growth environment (**Fig. 1**). The hydrothermal growth solution contained an equimolar concentration (40 mM) of zinc nitrate hexahydrate, hexamethylenetetramine (HMTA), and 7 mM polyethylenimine (PEI). The Au-coated PS MNs were suspended in the hydrothermal growth solution facing downward in the solution. The hydrothermal growth reaction was performed at 90 °C and in ambient pressure for 3 h. After the reaction, the MNs were removed from the solution and rinsed with deionized (DI) water and left to dry in a desiccator overnight. The morphology of ZnO nanobushes generated on Au-coated PS MNs was subsequently examined using scanning electron microscopy (SEM; JEOL JSM 6701F, Tokyo, Japan).

Mechanical Test and In Vitro Skin Penetration of ZnO-Coated PS MNs

The mechanical strength of MNs was examined using an Instron 5543 Tensile Meter (Instron, Norwood, MA). An MN patch was placed on a flat aluminum plate and an axial force was applied on a flat-headed stainless steel probe at a constant speed of 0.5 mm min^{-1} toward the MN tips placed facing upward on the flat aluminum plate. The displacement was measured until a preset maximum force of 0.8 N per tip was achieved. To evaluate the skin penetration efficiency, MNs were applied onto fresh porcine cadaver skin by thumb force for 2 min and removed. The skin tissue was then embedded in FSC22 Frozen Media (Leica Microsystem, Wetzlar, Germany) and cryosections (10 µm thick) were prepared using a cryostat (CM1950, Leica Microsystems). The skin sections were then stained with hematoxylin and eosin (H&E) for histological analysis. The removed MNs were examined using SEM to check the morphology changes of ZnO nanobushes on MNs.

Cell Viability Test

The influence of ZnO-coated PS MNs on cell viability was investigated using the AlamarBlue cell viability assay. Normal dermal fibroblasts (NDFs; 1×10^5 cells/cm^2) were preseeded in 24-well plates 24 h prior to the application of the ZnO-coated PS MNs. Subsequently, ZnO-coated PS MNs were applied to the cells in two configurations—direct contact with the needles and in the presence of MN but avoiding direct contact with the needles (see **Fig. 5A**). The cell culture was stored at 37 °C in a humidified environment containing 5% CO_2. NDFs not applied with ZnO-coated PS MNs were used as the positive control. After 24 h incubation with ZnO-coated PS MNs, the MNs were removed from the well plates and the AlamarBlue cell viability assay was performed according to the manufacturer's protocol

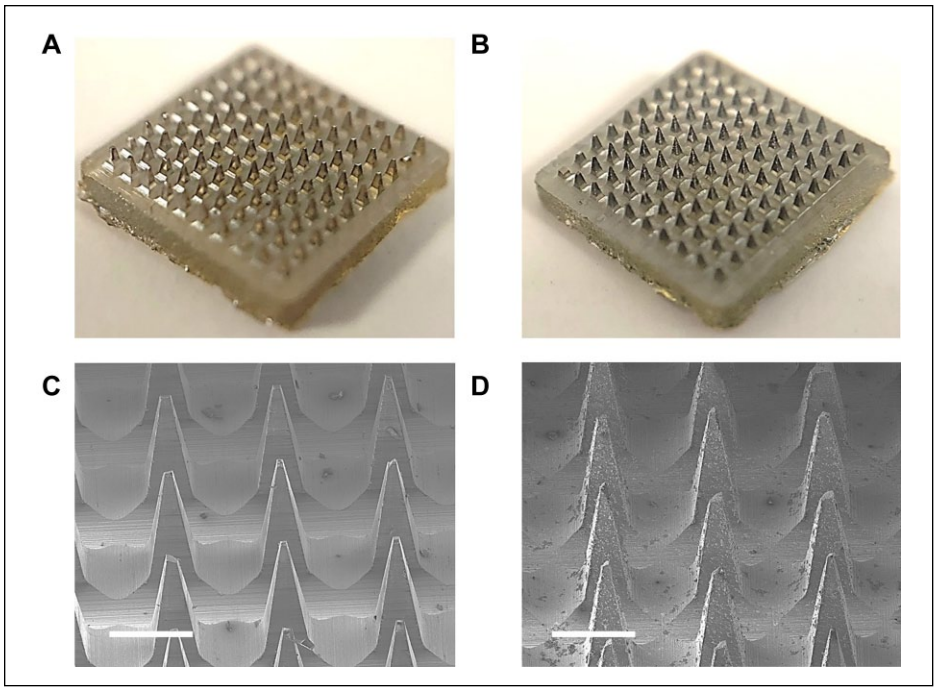

Figure 2. Optical images of (**A**) Au-coated PS MNs. (**B**) Au-coated PS MNs with ZnO nanobushes generated. (**C**) SEM images of Au-coated PS MNs. (**D**) Au-coated PS MNs with ZnO nanobushes generated. Scale bar = 500 μm.

(Invitrogen) and the absorbance of the incubated media containing 10% AlamarBlue (~8 h) was measured at 570 nm using a plate reader. The cell viability of the positive control was regarded as 100%, and the cell viability following application with ZnO-coated PS MNs was calculated by dividing the absorbance of experimental samples by the absorbance of the positive control. The test was performed in triplicate.

Agar Diffusion Assays

The antibacterial properties of MNs were evaluated using the agar diffusion assay protocol.[14] *S. aureus* ATCC 15981 and *S. enterica* subsp. *enterica* (ATCC, Manassas, VA) were cultured overnight in Luria–Bertani (LB) media in an incubator shaker at 37 °C. The bacterial cell suspensions were then centrifuged at 4000 rpm for 5 min. The bacterial cell pellet was then resuspended in 1× phosphate-buffered saline (Lonza, Basel, Switzerland) and diluted until the optical density at a wavelength of 600 nm was approximately 0.004. LB agar plates were inoculated with *S. aureus* and *Salmonella* using a sterile swab. Au-coated PS MNs with ZnO nanobushes were placed on the inoculated plates with the needles projecting into the agar. The inoculated plates were incubated at 37 °C for 24 h. The MN arrays were subsequently removed, and optical images were taken to determine the extent of bacterial growth. Each assay was carried out in triplicate and repeated thrice.

Results and Discussion

Fabrication and Characterization of Au-Coated PS MNs

PS MNs (**Fig. 2A**) made through the PDMS templating method have a height of approximately 650 μm with a base width of about 300 μm examined by SEM (**Fig. 2C**). The difference in dimensions of the MNs between PS MNs and the PDMS master template (base width = 300 μm; height = 1000 μm) is due to the shrinkage of the PDMS mold in the fabrication process after cooling from 240 °C heating. However, the MNs still demonstrated sharp tips and a well-replicated pyramid structure. The PS MNs were then coated with a 10 nm thick gold film using the thermal deposition method, which serves as a seed layer for the ZnO nanobushes to grow.[15]

Synthesis and Characterization of ZnO Nanobushes Deposited on Au-Coated PS MNs

The generation of ZnO structures via the hydrothermal growth method is well studied in the field of electronic device fabrication given its tunable electrical properties.[16] However, ZnO deposition via the hydrothermal growth method is mainly performed on flat surface substrates.[16–18] This paper carried out the first study on the generation of ZnO nanobushes on the MN 3D surface via the hydrothermal growth method.[19]

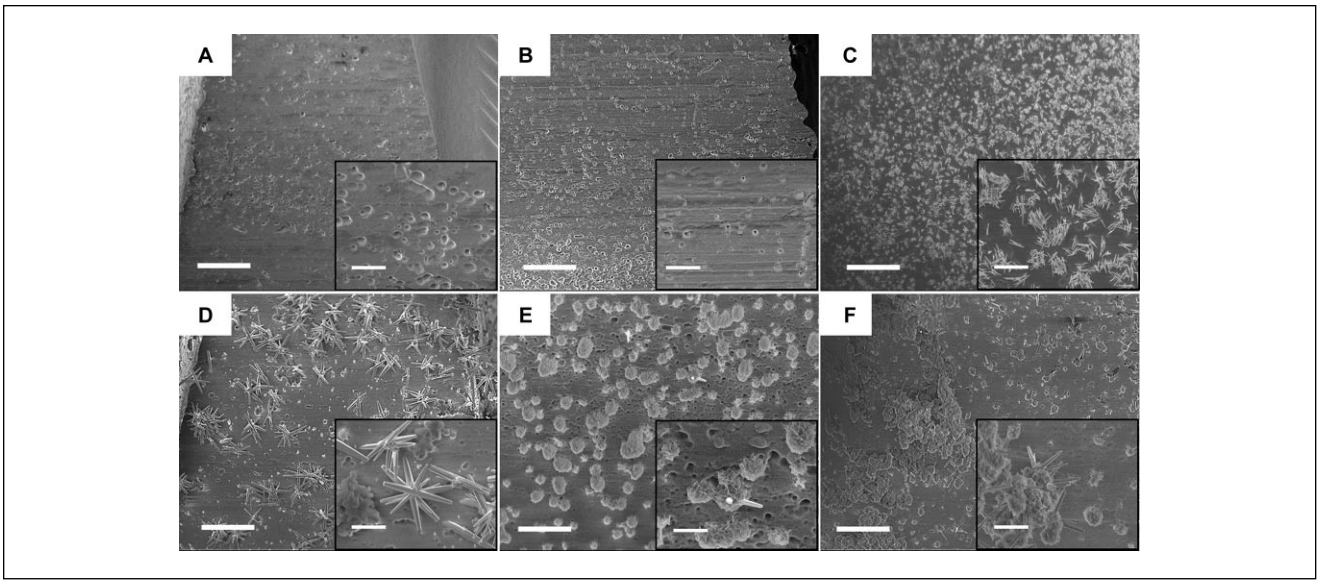

Figure 3. SEM images of ZnO nanobushes on Au-coated PS MN via the hydrothermal growth method with different precursor concentrations: (**A**) 10 mM, (**B**) 20 mM, (**C**) 30 mM, (**D**) 40 mM, (**E**) 50 mM, and (**F**) 60 mM. Insets show close-up views of the corresponding samples. Scale bars = 50 μm and 5 μm for the main images and insets, respectively.

Previous studies have shown that the concentration of the ZnO precursor is the key in controlling the morphology of the ZnO nanostructures.[15,16,18] Our study confirmed this (**Fig. 3**). When the precursor concentration was below 20 mM, no ZnO nanobushes were formed. The continuous increase of precursor concentration resulted in the deposition of ZnO nanobushes from thin, rodlike structures (30 mM) (**Fig. 3C**) to thicker nanopillar structures (40 mM) (**Fig. 3D**) to a mixture of nanobushes with rodlike structures (60 mM) (**Fig. 3F**).

Studies have shown that ZnO nanopillars could kill adhered bacteria through rupturing the bacterial cell wall by their rodlike structure.[20] Hence, we chose the rodlike ZnO nanobushes prepared by 40 mM precursor concentrations for the subsequent experiments (**Fig. 3D**). It is worth noting that the generation of ZnO nanobushes on the surface of Au-coated PS MNs did not show any noticeable change on the morphology of the MNs (**Fig. 2B,D**).

Skin Penetration Efficiency of ZnO Nanobush Decorated PS MNs

A plot of force versus displacement was obtained during the compression test to evaluate the mechanical strength of PS MNs before and after ZnO nanobush generation (**Fig. 4A**). None of the 100 MNs in the MN patch with and without ZnO nanobushes fractured during the compression testing. The 10 × 10 PS MN arrays were able to withstand an axial load of 80 N without fracture, and this corresponds to an axial load of 0.8 N per needle for both MN patches with and without ZnO nanobushes. These results suggest that the mechanical strength of the MN is not affected by the generation of ZnO nanobushes via the hydrothermal growth method.

The skin penetration capability of the MN patch was examined with fresh porcine cadaver ear skin. The MN patch easily perforated into the porcine ear skin by means of a thumb press force (approximately 1.5 N). A subsequent histology study showed successful penetration of the MN into the skin as indicated by the disruption of the stratum corneum, and the skin penetration depth was approximately 600 μm (**Fig. 4B,C**), which is slightly smaller than the actual length of PS MNs (i.e., 650 μm).

These results demonstrate that the mechanical property of MNs was affected by neither the hydrothermal growth reaction nor the ZnO nanobush generation on the surface, and the MNs were strong enough to penetrate the stratum corneum layer (~25 μm thickness) of the skin.

Cell Viability Test

Since the application of MN coated with ZnO nanobushes in skin results in contact with the skin tissue and cells, it is of great interest to study their influence on cell viability. NDFs were cultured with the MNs placed in different configurations. One group was cultured in the presence of the MNs but avoided direct contact with the needles (labeled as MN_top), which aimed to evaluate the intrinsic toxicity of the ZnO-coated PS MN patches. The other group was cultured in direct contact with the needles where the coating at ZnO nanobushes are present (labeled as MN_bottom). An overnight culture of the ZnO-coated PS MNs

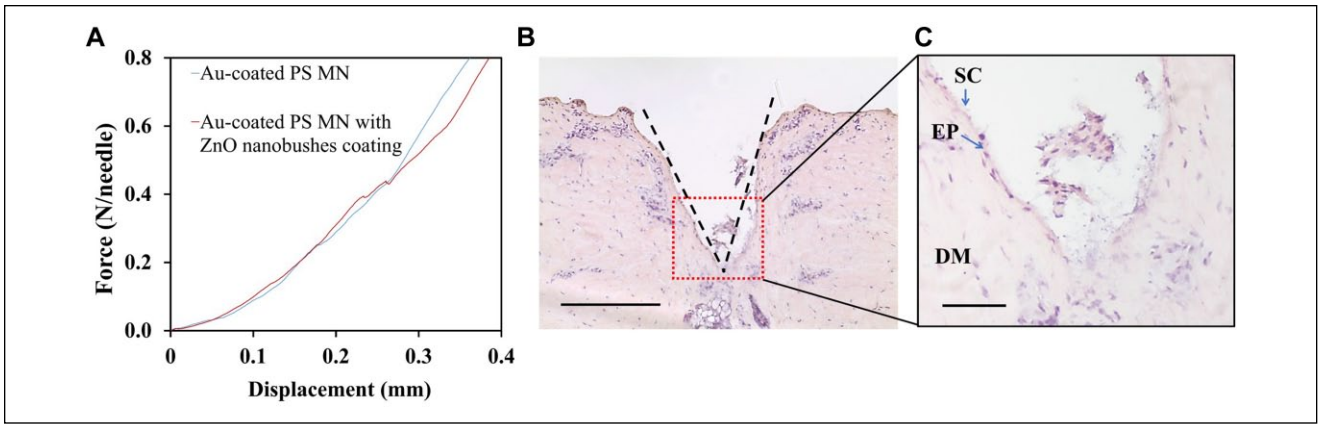

Figure 4. (**A**) Force–displacement curve of PS MNs with and without ZnO nanobush coating. (**B**) H&E-stained cross section image of porcine cadaver skin treated with PS MNs with ZnO nanobush coating. The region where MN insertion took place is outlined by the black dotted line. (**C**) Close-up image of the region of penetration of the MN and the structure of skin. SC = stratum corneum; EP = epidermis; DM = dermis. Scale bar = 500 μm.

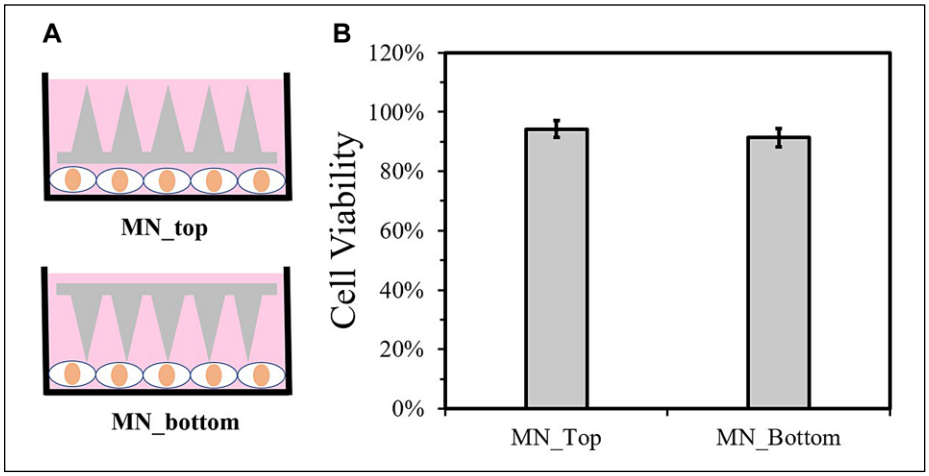

Figure 5. Cell viability test of NDFs with ZnO-coated PS MNs. (**A**) Schematic illustration of configuration of ZnO-coated PS MNs in the cell viability experiment. (**B**) Quantitative cell viability results of NDFs obtained from the AlamarBlue viability assay (n = 3).

with the cells showed no negative influence of the MNs on the cell viability (**Fig. 5B**). The viability of NDFs is 94% and 91%, respectively, for NDFs cultured in the presence of MN without direct needle contact and NDFs cultured in direct contact with the needles of MN after normalization with control. This demonstrates the biocompatibility of the ZnO-coated PS MNs for application in skin.

Antibacterial Activity of MN

Finally, the antimicrobial property of MNs with ZnO nanobush modifications was investigated using the agar diffusion assays with gram-positive *S. aureus* and gram-negative *Salmonella* (**Fig. 6A–D**). The protocol is commonly used to assess the growth of pathogenic microorganisms through providing qualitative data on the susceptibility of the microorganism to an antimicrobial agent.[14] When the plate was covered with bare MNs without ZnO nanobushes, both *S. aureus* (**Fig. 6A**) and *Salmonella* (**Fig. 6C**) could be observed in large plaques around the MN tips. In comparison, when the agar plate was covered with MNs with ZnO nanobushes, there was neither *S. aureus* (**Fig. 6B**) nor *Salmonella* (**Fig. 6D**) growth around the MN tips. The quantification using ImageJ based on intensity and size (**Fig. 6E**) showed that the ZnO nanobushes decreased the bacterial colony number in the area covered by MN patches by approximately 85.6%. The possible mechanism behind the antibacterial activity could be due to the rupturing of the bacteria cell by the rodlike structure of the ZnO nanobush coating shown in **Figure 3D**. As mentioned earlier, the literature has shown that ZnO nanofeatures can kill bacteria through rupturing the bacterial cell wall by their rodlike structure.[20] However, the employment of ZnO nanobushes generated on an MN 3D surface for antibacterial activity is

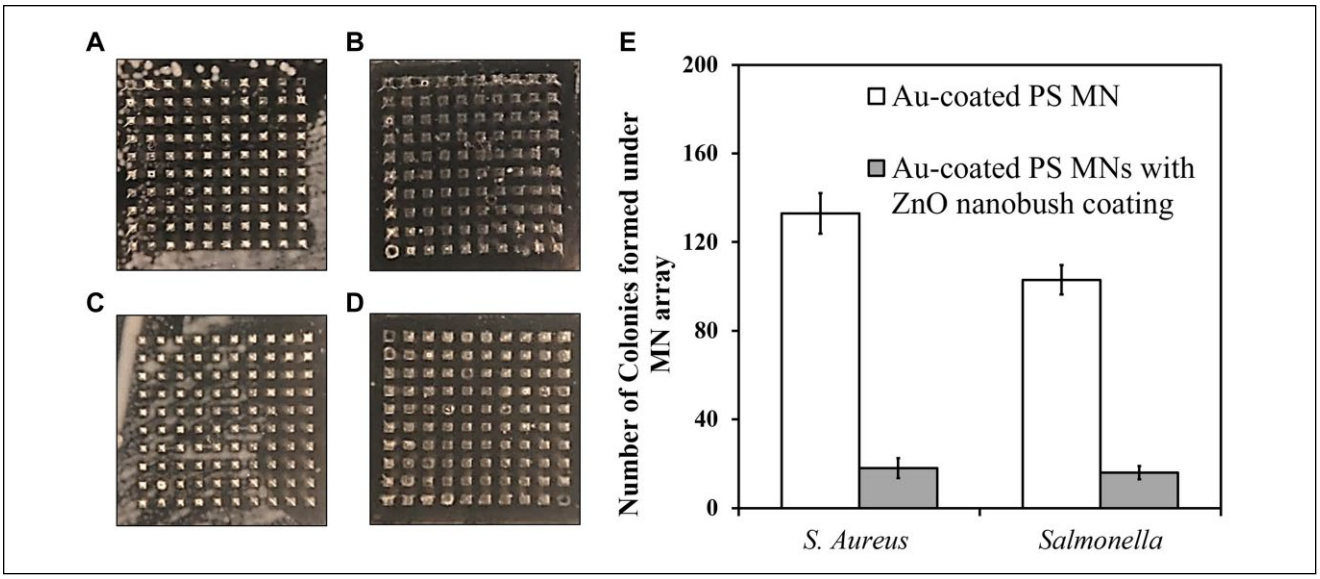

Figure 6. Agar diffusion assay results of (**A**) *S. aureus* ATCC 15981 with Au-coated PS MNs as the control, (**B**) *S. aureus* ATCC 15981 with Au-coated PS MNs with ZnO nanobush coating, (**C**) *Salmonella* with Au-coated PS MNs as the control, and (**D**) *Salmonella* with Au-coated PS MNs with ZnO nanobush coating. (**E**) Number of colonies formed under the MN array quantified using ImageJ. Error bar represents SD.

the first to be reported in this paper; future studies exploring the different parameters of ZnO-coated PS MNs, including the density and thickness of the ZnO coating and size and shape of the MN patch, can be performed to elucidate the mechanism behind the antibacterial activity of ZnO-coated PS MNs and their influence on the antibacterial activity.

This report has introduced a facile method to fabricate MNs with an antimicrobial coating via the in situ generation of ZnO nanobushes. Different ZnO nanobushes were prepared with the hydrothermal growth method by tuning the precursor concentration. An agar diffusion assay demonstrated the antimicrobial capability of the MNs through successful inhibition of the growth of both gram-positive and gram-negative bacteria. This study used PS MNs as the example to demonstrate the deposition of the antibacterial coating. This strategy is not limited to PS MNs, however; it can be extended to MNs made from other materials. With this method, MNs of various materials can be incorporated with antimicrobial functionality, and this can greatly increase the utilization of MN technologies in clinical settings.

Declaration of Conflicting Interests

The authors declared no potential conflicts of interest with respect to the research, authorship, and/or publication of this article.

Funding

The authors disclosed receipt of the following financial support for the research, authorship, and/or publication of this article: This work was supported by Singapore A*STAR Biomedical Research Council (IAF-PP grant), NTU SUG (M4082114), and the Primary Research & Development Plan of Jiangsu Province of China (BE2016770). The thermal evaporator was supported by the Center for Disruptive Photonic Technologies of NTU.

References

1. Bhatnagar, S.; Dave, K.; Venuganti, V. V. K. Microneedles in the Clinic. *J. Control. Release* **2017**, *260*, 164–182.
2. Wang, M.; Hu, L.; Xu, C. Recent Advances in the Design of Polymeric Microneedles for Transdermal Drug Delivery and Biosensing. *Lab Chip* **2017**, *17*, 1373–1387.
3. Prausnitz, M. R.; Langer, R. Transdermal Drug Delivery. *Nat. Biotechnol*. **2008**, *26*, 1261–1268.
4. Than, A.; Liang, K.; Xu, S.; et al. Transdermal Delivery of Anti-Obesity Compounds to Subcutaneous Adipose Tissue with Polymeric Microneedle Patches. *Small Methods* **2017**, *1*, 1700269.
5. Ye, Y.; Wang, C.; Zhang, X.; et al. A Melanin-Mediated Cancer Immunotherapy Patch. *Sci. Immunol*. **2017**, *2*, eaan5692.
6. Kim, Y. C.; Park, J. H.; Prausnitz, M. R. Microneedles for Drug and Vaccine Delivery. *Adv. Drug Deliv. Rev*. **2012**, *64*, 1547–1568.
7. Birchall, J. C. Microneedle Array Technology: The Time Is Right but Is the Science Ready? *Expert Rev. Med. Devices* **2006**, *3*, 1–4.
8. Kalia, Y. N.; Nonato, L. B.; Lund, C. H.; et al. Development of Skin Barrier Function in Premature Infants. *J. Invest. Dermatol*. **1998**, *111*, 320–326.
9. Gittard, S. D.; Ovsianikov, A.; Akar, H.; et al. Two Photon Polymerization-Micromolding of Polyethylene Glycol-Gentamicin Sulfate Microneedles. *Adv. Eng. Mater*. **2010**, *12*, B77–B82.

10. Gittard, S. D.; Narayan, R. J.; Jin, C.; et al. Pulsed Laser Deposition of Antimicrobial Silver Coating on Ormocer Microneedles. *Biofabrication* **2009**, *1*, 041001.
11. Gittard, S. D.; Miller, P. R.; Jin, C.; et al. Deposition of Antimicrobial Coatings on Microstereolithography-Fabricated Microneedles. *JOM* **2011**, *63*, 59–68.
12. Boehm, R. D.; Miller, P. R.; Singh, R.; et al. Indirect Rapid Prototyping of Antibacterial Acid Anhydride Copolymer Microneedles. *Biofabrication* **2012**, *4*, 011002.
13. Park, S. Y.; Lee, H. U.; Lee, Y. C.; et al. Wound Healing Potential of Antibacterial Microneedles Loaded with Green Tea Extracts. *Mater. Sci. Eng. C Mater. Biol. Appl*. **2014**, *42*, 757–762.
14. Kiehlbauch, J. A.; Hannett, G. E.; Salfinger, M.; et al. Use of the National Committee for Clinical Laboratory Standards Guidelines for Disk Diffusion Susceptibility Testing in New York State Laboratories. *J. Clin. Microbiol*. **2000**, *38*, 3341–3348.
15. Lopez, O. E.; Tucker, A. L.; Singh, K. R.; et al. Synthesis of Zinc Oxide Nanowires on Seeded and Unseeded Gold Substrates: Role of Seed Nucleation and Precursor Concentration. *Superlattices Microstruct*. **2014**, *75*, 358–370.
16. Boubenia, S.; Dahiya, A. S.; Poulin-Vittrant, G.; et al. A Facile Hydrothermal Approach for the Density Tunable Growth of ZnO Nanowires and Their Electrical Characterizations. *Sci. Rep*. **2017**, *7*, 15187.
17. Bielinski, A. R.; Boban, M.; He, Y.; et al. Rational Design of Hyperbranched Nanowire Systems for Tunable Superomniphobic Surfaces Enabled by Atomic Layer Deposition. *ACS Nano* **2017**, *11*, 478–489.
18. Xu, S.; Lao, C.; Weintraub, B.; et al. Density-Controlled Growth of Aligned ZnO Nanowire Arrays by Seedless Chemical Approach on Smooth Surfaces. *J. Mater. Res*. **2011**, *23*, 2072–2077.
19. Xiao, X.; Yuan, L.; Zhong, J.; et al. High-Strain Sensors Based on ZnO Nanowire/Polystyrene Hybridized Flexible Films. *Adv. Mater*. **2011**, *23*, 5440–5444.
20. Yi, G.; Yuan, Y.; Li, X.; et al. ZnO Nanopillar Coated Surfaces with Substrate-Dependent Superbactericidal Property. *Small* **2018**, *14*, e1703159.